Pergamon

Journal of Structural Geology, Vol. 19, No. 10, pp. 1257 to 1271, 1997

PII: S0191-8141(97)00041-2
0191-8141/97 $17.00 + 0.00

Scaling and connectivity of joint systems in sandstones from western Norway

NOELLE E. ODLING

NERSC, Edvard Greigsvei 3A, N-5037 Solheimsviken, Bergen, Norway

(*Received* 10 *June* 1996; *accepted in revised form* 25 *April* 1997)

Abstract—The scaling properties of a joint system in Devonian sandstones in western Norway have been investigated using seven maps, covering areas from 18 to 720 m across, which were generated by mapping in the field and from low-level aerial photography taken from different heights. Each map represent a scale 'window' on the fracture population, bounded by resolution at small scales and the sample size at large scales. A power-law relationship between fracture trace length and critical observation height (maximum height at which a trace can be identified) is derived and used to create a statistical model for the resolution effects. The model indicates that a continuous smooth curve without a straight-line segment on a log–log cumulative frequency distribution plot does not necessarily rule out a power law as the underlying population distribution. Together, the maps indicate a power-law trace-length distribution with an exponent of −2.1. This power law may be valid over four or more orders of magnitude, with natural lower cut-off of around 1 m. The exponent is significantly different from −2.0 (strictly self-similar case) and is reflected in a decrease in the abundance of fractures with length comparable to map size, as map scale decreases. The fracture trace-length distribution results in a decrease in apparent connectivity, with decreasing scale. High resolution (large-scale) maps are well connected while the lowest resolution map (smallest scale) is unconnected. Fractures in the smallest scale map are, however, connected by small fractures below the limit of resolution, represented by the largest scale map. The variation in apparent connectivity with scale has implications for fluid flow. When fractures are open to fluid flow the scaling properties of apparent connectivity imply that, beyond a certain scale, the size of fracture controlling flow will be scale-independent. In this fracture system, this appears to occur in sample areas of around 300 m across. © 1997 Elsevier Science Ltd.

INTRODUCTION

Joints are a very common feature of the upper portions of the Earth's crust, occurring on a wide range of scales from microjoints on the scale of mineral grains to 'master' joints many kilometres in length. The presence of joints has important effects on the mechanical properties and permeability of rock masses. From an engineering point of view, joint systems strongly influence rock-mass stability and strength. Much research into flow and contaminant transport in fractured rocks has been motivated by the problems of hazardous waste disposal in fractured hard-rock terrains and recovery of hydrocarbons from fractured reservoirs (e.g. Van Golf-Racht, 1982; Long and Witherspoon, 1985; Herbert and Splawski, 1990). These applications have motivated extensive work on the characterization of joint systems (e.g. Hancock, 1985; La Pointe and Hudson, 1985; Heffer and Bevan, 1990), and on the simulation of fracture systems (e.g. Long *et al.*, 1982; Billaux *et al.*, 1989).

The importance that fracture systems have for rock-mass properties depends on properties associated with individual fractures (e.g. orientation, size, aperture), and on properties associated with the fracture system as a whole (fracture density, geometry of the fracture network). In addition, changes in these properties with scale are crucial to the prediction of large-scale properties from small-scale observations. Many workers have remarked on the apparent 'self-similarity' of fault and fracture systems, i.e. that fracture patterns at different scales appear qualitatively similar. In recent years, there has been an increasing number of studies into fracture size and fault-displacement scaling. However, scaling of other fracture system properties and implications for engineering and hydrogeological applications are at present little understood.

In this paper the scaling of a joint system from Devonian sandstones in western Norway on scales from metres to kilometres is described. The area was chosen primarily because exposure is unusually good, and because the geology and tectonic history of joint formation are relatively simple, facilitating an understanding of the joint systematics and their scaling behaviour. The properties of this joint system are investigated through a series of fracture maps representing the joints at different scales. These fracture maps have been constructed from mapping in the field and from aerial photographs taken from a variety of observation heights. They are used to determine to what extent the scaling of the fracture system obeys identifiable laws and can therefore be considered predictable, if these laws are known.

THE DATA

The Devonian basin of Hornelen, western Norway

The fracture system studied occurs in Devonian-age sandstones of Hornelen in western Norway, approximately 200 km north of Bergen (Fig. 1). In Hornelen, sandstones and conglomerates fill a fault-bounded basin, approximately 70 × 30 km in extent, which is the remnant of a once much larger basin (e.g. Norton, 1986). The

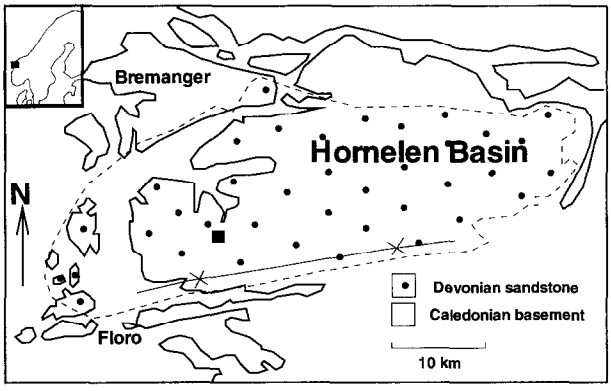

Fig. 1. Map of Hornelen basin, western Norway, showing the extent of Devonian rocks (largely sandstones) and location of the study area (filled square).

basin sediments (largely sandstones) form laterally continuous cycles on the order of 100–200 m thick and composed of beds around 2 m thick. The sedimentary layering has an overall dip of approximately 15°E. The cycles are generally marked by a finer-grained portion at their base (R. Steel, personal communication) and they impose a very strong control on topography, which consists of E-facing slopes parallel to the tops of the cycles and separated by cliffs. Slopes on the tops of the cycles are steep enough to be avalanche prone in winter, which keeps them to a large extent free of vegetation, resulting in large areas of excellent exposure, ideal for the study of joint systematics and scaling.

The rocks are little deformed apart from open to gentle folds with E–W-trending axes at the present-day basin margins; the folds are thought to have developed during Late Caledonian compression (Steel, 1976). The rocks have suffered metamorphism bordering on greenschist grade (e.g. Wilks and Cuthbert, 1994) and now have very low permeability (0.02 mD, Mæhle, 1975). Joints perpendicular to the bedding are common throughout the basin, while faults showing significant shear displacement, with the exception of the bounding faults, are rare. Earliest identifiable fractures are mineral-filled breccia zones which are cut by later straight veins. Both these types of fracture are cut by unfilled joints. This suggests a history of fracturing which spans a range of pressure and temperature conditions. Jointing intensity increases towards the boundary faults, correlating with fold shortening. Joint orientations are generally symmetrically disposed about the fold axis. The relative timing of folding and fracturing is uncertain, but this correlation suggests that the same stress system controlled both structures. Sandstone fragments embedded in the mineral fill of breccia zones have similar porosity to that of the country rock, suggesting that the fracturing history began after the rocks had been buried to their maximum depth. Thus, the most probable explanation of joint development in the area is as a response to stress release on uplift (e.g. Price, 1966; Nur, 1982). The latest-formed unfilled joints are by far the most common, and also those most visible. This study concentrates on these latest joints.

Collection methods

A series of joint maps was constructed from data collected on the top surface of a sedimentary cycle using mapping in the field and from low-level aerial photographs taken from a range of observation heights. In the case of the highest resolution map, a grid of 2 m cells was marked out in an area of 18 × 18 m, and the fracture patterns were drawn onto squared paper from a standing position (i.e. an observation height of 1.5 m). For the aerial photography, a series of crosses ranging in size from 0.2 to 8 m across were painted on the rock surface to assist later assembly. Photographs were taken: (a) from a 35 mm camera with 50 mm lens suspended from helium-filled balloons at heights of 10 and 20 m above the rock surface; and (b) from a helicopter using a medium format camera with an 80 mm lens at four observation heights ranging from 35 to 368 m.

A series of maps of the fracture system were generated from the photographic surveys. Each map was constructed from a number of photographs, 121 in the case of the 35 mm camera, and 16 in the case of the 80 mm medium format camera. It was found impractical to ensure a normally incident viewing direction during the photographic surveys and most of the aerial photographs were thus slightly oblique. Before assembly, the images were rectified using a perspective transformation (e.g. Burnside, 1979) with additional minor corrections using the reference crosses as calibration points. Each map was digitized and fracture trace junctions automatically controlled using an estimated digitizing error equal to the map-line thickness. This ensures that the connectivity of the original map is correctly represented in the digitized data. A total of seven fracture maps were generated using the above methods. The maps, their sizes, collection methods and observation heights are listed in Table 1, and their relative locations are shown in Fig. 2. Three examples of the maps are shown in Fig. 3.

Photographic resolution

It is clear from observations of outcrop surfaces that the visual signature of fracture traces varies, i.e. some are clearly discernible while others are faint. Visual signature controls the maximum possible distance of an observer from the surface while still able to detect the trace. Any fracture map, therefore, represents a 'window' or subsample of the fracture trace population with a lower bound controlled by the resolution of the mapping method (fracture traces too faint to see are not recorded), and an upper bound controlled by the size of the region observed (fracture traces of length similar to the sampled region or larger are censored and therefore badly sampled). These two factors control the fractures observed regardless of the viewing distance.

Table 1. Details of the fracture maps. Normalized observation heights are the equivalent heights for the same image when a lens with a focal length of 80 mm is used. These are calculated using simple geometrical arguments from $D' = f'D/f$, where D is the observation height, D' is the normalized observation height, f is the actual focal length and f' is a focal length of 80 mm

Map	Method	Area (m^2)	Focal length (f) (mm)	Observation height (D) (m)	Normalized observation height (D') (m)
1	Hand-mapping	18 × 18	30	1.5	4
2	Balloon survey	55 × 55	50	10	16
3	Balloon survey	90 × 90	50	20	32
4	Helicopter survey	90 × 90	80	35	35
5	Helicopter survey	180 × 210	80	80	80
6	Helicopter survey	360 × 360	80	160	160
7	Helicopter survey	720 × 720	80	368	368

The images used to generate the fracture trace maps were generated by eye and photographic means. These two methods are similar in that they use approximately the same range of light wavelengths to create an image. For a given observation distance, the nature of the image is affected by many factors, including the direction of the sun and atmospheric conditions, film sensitivity (retina sensitivity), and lens focal length and quality. The aerial photographs were taken in lightly overcast conditions with no direct sunlight on the rock surface so that directionally dependent shadows were minimal. As the viewing distances were no greater than 400 m, and the weather during photography was clear, the atmospheric effects can be assumed to be constant. Tests on the two film types used showed that the differences in film sensitivity were minimal. The difference in lens quality of the cameras used is also negligible. The focal lengths of the lenses, however, were different (50 and 80 mm). For a given observation height, the focal length controls the amount of information on the ground which is transferred to a unit area of negative, and thus controls the resolution of the image. Resolution is therefore considered to be primarily controlled by the observation height and the focal length of the camera lens. In order to compare the different maps, the observation heights were standardized to a focal length of 80 mm (that of the medium format camera), and these standardized observation heights are listed in Table 1.

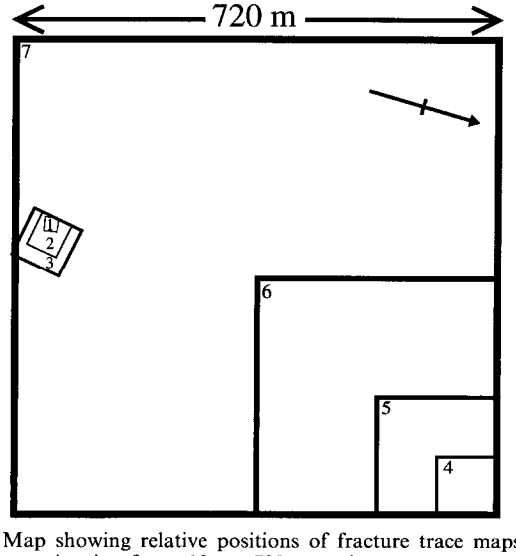

Fig. 2. Map showing relative positions of fracture trace maps 1–7. Maps range in size from 18 to 720 m and represent a range of resolutions. The arrow points north.

Calibration

To investigate what controls the visual signature of fracture traces and to calibrate the resolution of the photographs, the nature of the faintest fracture trace at each observation height was examined on the ground. At the highest resolution (hand-mapped regions), the faintest traces are hair-line fractures made visible by deposits of fine soil and black algae which create a thin dark line, 0.1 mm broad or less, along the line of the trace. As observation height increases the faintest traces increase in width to approximately 1 mm until, at an observation height of 80 m, the faintest trace is no longer a single discontinuity, but two or three parallel fractures with spacings of 1–2 mm. Fracture-bounded blocks of rock within the central portion have frequently been removed (by glacial action) to create depressions of width and depth up to 1 cm. The bottoms of these depressions contain fine soil particles, moss and algae, making them considerably darker than the surrounding rock. As the observation height increases further, the faintest fracture traces correspond to fracture zones composed of increasing numbers of parallel fracture traces. Cross-fractures divide the zones into blocks that in many places have been removed by glacial action. At the greatest observation height of 368 m, the faintest fracture trace corresponds to a depression 30 cm across which is locally filled with soil, grass or water.

Figure 4 illustrates the effects of resolution on the observed fracture pattern of a specific area. With increasing observation height, short fracture traces are progressively removed as they fall below the limit of resolution. In addition, complex structures of closely spaced and en échelon traces merge to form single traces. Thus, decreasing resolution results in a thinning out and a simplification of the observed fracture network. This illustrates an important feature of the fracture network. The joint system is composed of a complete gradation of

MAP 1: H = 4m, Area = 18 x 18m

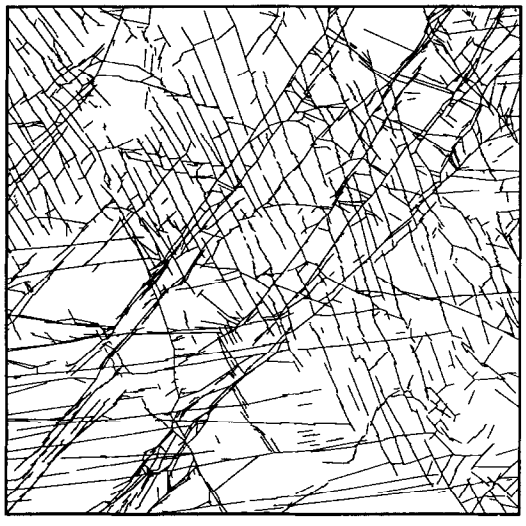

MAP 4: H = 35m, Area = 90m x 90m

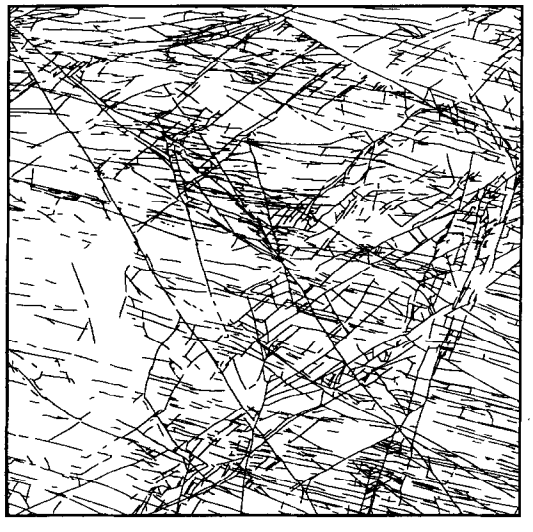

MAP 7: H = 370m, Area = 720m x 720m

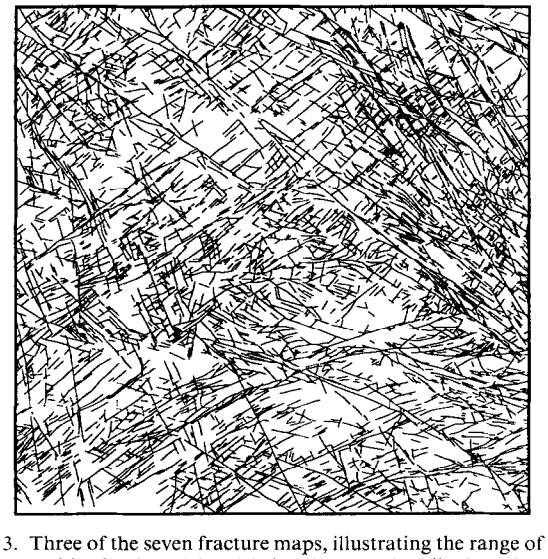

Fig. 3. Three of the seven fracture maps, illustrating the range of scales represented in the data. Map 1 is hand-mapped while the others were constructed from aerial photographs. Their relative positions and orientations are shown in Fig. 2. *H*, observation height.

features from single joints to large-scale zones which are complex structures composed of many fractures. Ground observation shows that fractures making up these zones are also joints, i.e. display no significant shear displacement. It is therefore reasonable to assume that the joint zones represent large-scale joints and have the same physical origin as the smaller-scale features. This organization of the fracture system into large- and small-scale features has important consequences for the properties of fractured rock masses.

If it were possible to map the entire study area at the highest (field-scale) resolution individual joints in joint zones would be recorded and no individual joints longer than a few tens of metres would be found. A statistical analysis of the length distribution in such a map would, however, fail to capture the spatial organization of the joint system. A rough calculation shows that such a map would contain over four million fracture traces, clearly an impossible mapping task. By using the resolution of the camera at different observation heights to select subsets of the fracture population, the problem is rendered tractable, and important aspects of joint system structure are captured.

DATA ANALYSIS

Joint orientation

The fracture trace maps (Fig. 3) show that fracture traces tend to occur in sets of preferred orientation. The mean orientations characterizing each set were identified in each map by determining the best-fit mixed Von Mises distribution (e.g. Cheeney, 1983). Given the number of fracture sets expected, the method is used to determine the mean orientation and other parameters (amplitude and standard deviation) of each set, and the fit between the estimated theoretical and observed distributions is tested using the Kuiper test (e.g. Cheeney, 1983). With such a method, it is always possible to get a better fit to the data by increasing the number of expected orientation sets. However, beyond a certain number this is not useful as it only serves to reproduce noise in the data. Thus, the minimum number of sets that gave a statistically acceptable fit (Kuiper test at the 0.01 level of significance) was used to characterize the orientation distribution. This procedure gave similar results to that expected by a visual inspection of the fracture trace maps and gave a good visual fit to the frequency distributions (Fig. 5).

A maximum of four orientation sets was identified in the individual maps, and three of these four sets could be identified on all maps (mean set orientations 0°, 50° and 130°). There is good correspondence between the mean set of orientations from map to map (Fig. 5). For a given orientation set, frequency peak heights appear to vary fairly smoothly from one scale to the next, but maximum peak heights occur at different scales for different fracture sets. The fracture system therefore appears to be self-

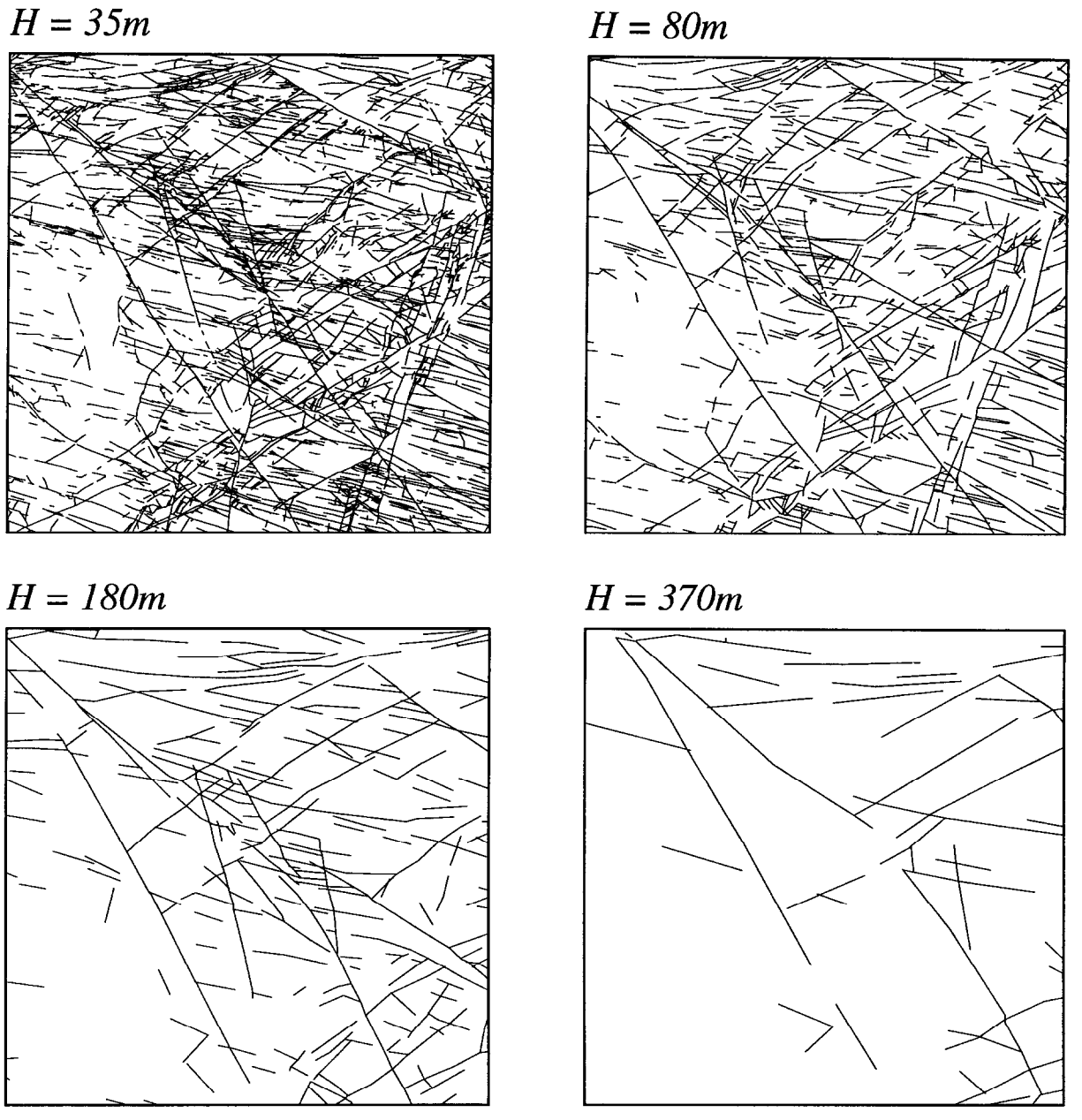

Fig. 4. The effects of resolution on the observed fracture pattern in an area 90 x 90 m, shown by map 4 (upper left), part of map 5 (upper right), part of map 6 (lower left) and part of map 7 (lower right). As resolution (and observation height) decreases, short fracture traces are lost and complex structures of closely spaced and en échelon traces merge to form single traces.

similar with respect to mean fracture orientation (i.e. mean set orientations are scale-independent), but not with respect to the relative abundance of fractures of the various sets, which is not readily predictable.

Fracture trace-length distribution

The trace-length distributions of individual maps were found to be log-normal or close to log-normal (Kolmogorov–Smirnof test at the 0.01 level of significance). In most cases, the difference in length distribution between orientation sets was found to be insignificant. To look at the system as a whole, cumulative distributions of fracture traces per km^2 were plotted (log–log) against fracture trace length (Fig. 6). Such plots have been extensively presented in recent literature on the scaling of fracture-length distributions (e.g. Heffer and Bevan, 1990; Yielding *et al.*, 1992). The positions of individual log-normal distributions, which appear as curves on Fig. 6, confirm that as observation height increases the window of observation moves to larger trace lengths. Collectively, the curves are bounded by a straight line with a negative slope, suggesting that the parent population is governed by a power law. The curvature of individual distributions is attributed to a combination of truncation (short trace lengths are inadequately

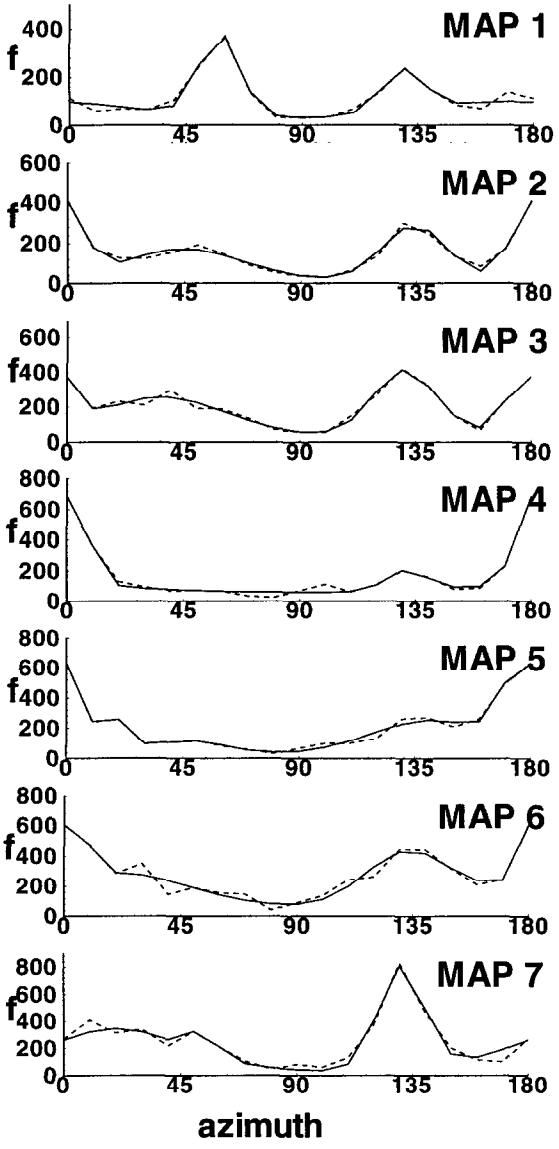

Fig. 5. Frequency of fracture traces per 10° interval of azimuth for each of maps 1–7. Each map represents a different scale interval of the total fracture population. Solid line, observed orientation frequency distribution; dotted, best-fit mixed Von Mises distribution. The maps contain three main orientation sets indicated by the peaks in the frequency distributions. There is good correspondence in the mean orientation of sets (peak locations) from one scale to another, but the relative abundance of the sets (peak heights) is unpredictable.

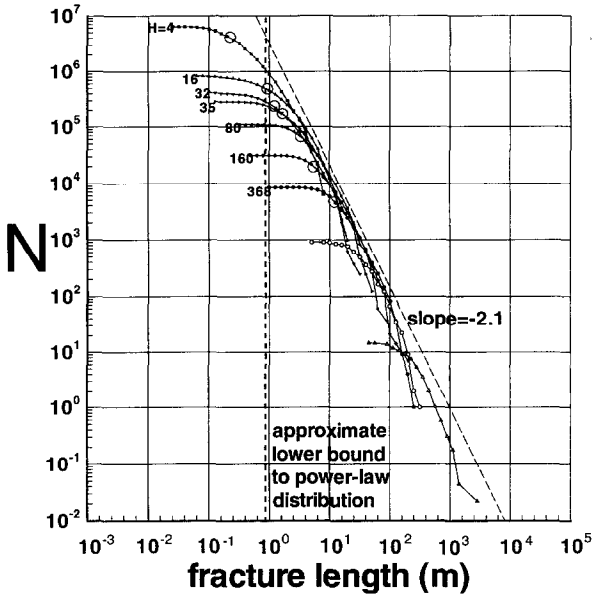

Fig. 6. Cumulative frequency per km^2 of fracture trace length for maps 1–7, representing different scale ranges of the fracture system. Together the distributions describe an envelope (dashed line) that indicates a power-law parent distribution with an exponent (slope of the graph) of −2.1. (This line has been displaced slightly to the right for clarity of the plot.) Individual samples show log-normal distributions, the mode of which is indicated by open circles. Semi-quantitative considerations suggest a natural lower cut-off to the power law at around 1 m. Additional data from state aerial photographs (open symbols) indicate that the power law may be valid up to scales of several kilometres.

resolved) and censoring effects (long traces are inadequately sampled).

To investigate the validity of this power law further, and to quantify its slope, the effects of truncation and censoring are more closely examined. While methods for correcting censoring are described in the literature, techniques for correcting truncation (resolution) effects are not so readily available and most authors assume that the section of the observed population affected by resolution has been removed from the sample before an analysis is made. For individual samples, the point at which a straight-line segment begins on the log–log cumulative frequency plot was taken as the limit of truncation effects. Cut-off lengths correspond to between 5 and 10% of the map size. Cut-off points were easiest to identify in the small-scale (lower resolution) maps which show more clearly defined straight-line segments. Inclusion of data points still significantly affected by resolution will tend to reduce estimated slope steepness on a log–log cumulative distribution plot.

After removal of points significantly affected by truncation (resolution), the curves were corrected for censoring (finite sample size effects). The Kaplan–Meier method (Cox and Oakes, 1984; Lindsay and Rothrock, 1995), which is a non-parametric method and therefore does not depend on the underlying distribution, was used. In this method, the Kaplan–Meier or product-limited estimation $F(l)$ of the cumulative distribution function gives the proportion of traces greater or equal to trace length, l:

$$F(l) = \prod_{k \le l} \left[1 - \frac{N_f(k)}{r(k)} \right] \quad (1)$$

where

$$r(k) = \left[\sum_{l=k}^{L} [N_f(l) + N_p(l)] \right] - \frac{1}{2} N_p(k) \quad (2)$$

where $N_f(l)$ is the number of fully observed (uncensored) fracture traces and $N_p(l)$ is the number of partially observed (censored) fracture traces of length, l. Censored and uncensored traces are counted separately and

binned, using linear bins, to form $N_f(l)$ and $N_p(l)$ which are then used in the above equations.

A test of the method was performed using cases in which both the truncated and untruncated populations are known. The first is the highest resolution map (map 1), where all fractures in the sample area were mapped to their ends. A second untruncated population was created from the lowest resolution map (map 7) by moving all boundaries inwards (reducing the map area) until the untruncated lengths of all fracture traces within the remaining area are known. Comparing the truncated and untruncated length data with the corrected truncated samples (Fig. 7a) shows that the corrected data follow the untruncated sample closely over most of the range. Applying the method to the trace-length samples from the seven maps showed that slope estimates became less steep by between 0.2 and 0.8.

An additional possible source of error lies in the location of the study area. The study area was chosen as one of the largest areas of continual exposure available in the region. The largest fractures in the region form features 10 km long or more which form grassy gullies tens of metres wide. On the scale of the study area (720 × 720 m) such features constitute areas of poor exposure and were avoided. This means that the largest fractures found in the region as a whole are missing from the study area. This differs from censoring effects, as it is caused by the manner in which the study area is chosen. Such sampling problems cause right-hand 'fall-off' of the curves on a log–log cumulative distribution plot (Pickering *et al.*, 1995). The method of Pickering *et al.* (1995) corrects for such effects by increasing the observed frequency of the largest fracture class until the best fit to a straight line (power law) is obtained. This correction was applied to the trace-length data after correction for truncation and, in all except one case, the frequency of the largest fractures were incremented by 5 or less. This correction also reduces slope steepness, and modifies the estimated slopes of individual samples by a further 0.2–0.7. The effect of both corrections is shown for the example of map 7 in Fig. 7(b). It can be seen from Fig. 7(b) that the censoring corrections are larger than sampling error adjustments.

The trace-length distributions from the seven maps, corrected for truncation and sampling error using the above methods, are shown in Fig. 8. The samples together indicate a power-law distribution extending over two orders of magnitude. Taken together, the data give a slope estimate of −2.2 (fit by minimum absolute deviations, Press *et al.*, 1992). Individually, the samples give best-fit straight lines with slopes between −1.9 and −2.4 and show no correlation with map scale. The spread in individual sample slopes illustrates the difficulty in determining a representative power-law exponent from limited scale-range data.

An alternative to correcting individual samples, is to consider the original samples collectively. Some part of each sample reflects the underlying power-law distribution, although this part may be small. These parts lie along or close to the straight line which forms an upper bound or envelope to the curves on a log–log cumulative distribution plot (see Fig. 6). An estimate of slope was made by determining this envelope straight line by the following method. An initial guess at the parent power-law distribution slope is made. The point on each curve at which this line is tangential is identified. The line is then shifted parallel to the Y-axis, maintaining its slope, until the best fit to these tangent points is found. The summed perpendicular distances of the points to the line then represent a measure of the goodness of fit of the line as an

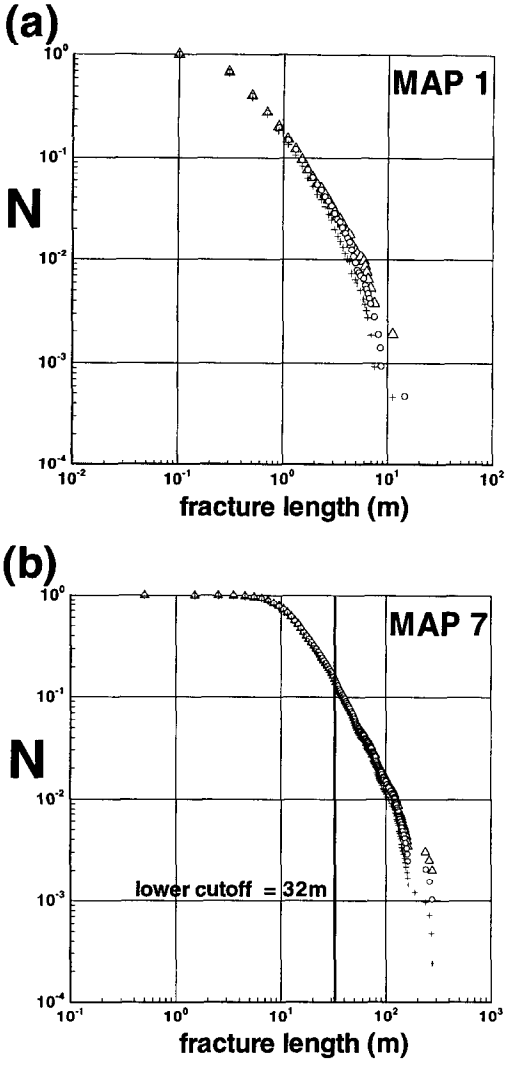

Fig. 7. (a) Normalized cumulative frequency distribution of fracture trace lengths in map 1 showing correction for truncation effects using the Kaplan–Meier method. Crosses, observed truncated sample; circles, observed untruncated sample; triangles, truncated sample after correction. The observed and corrected samples agree well. (b) Cumulative frequency distribution of fracture trace lengths for map 7 showing corrections for truncation and finite sample size effects. Crosses, original data; circles, after correction for truncation effects (Kaplan–Meier method); triangles, after additional corrections for finite sample size effects (method of Pickering *et al.*, 1995). After a lower cut-off of 32 m was applied to remove resolution effects, slope estimates were: the original data −2.9; after correction for truncation −2.4; and after additional corrections for finite sample size effects −2.1.

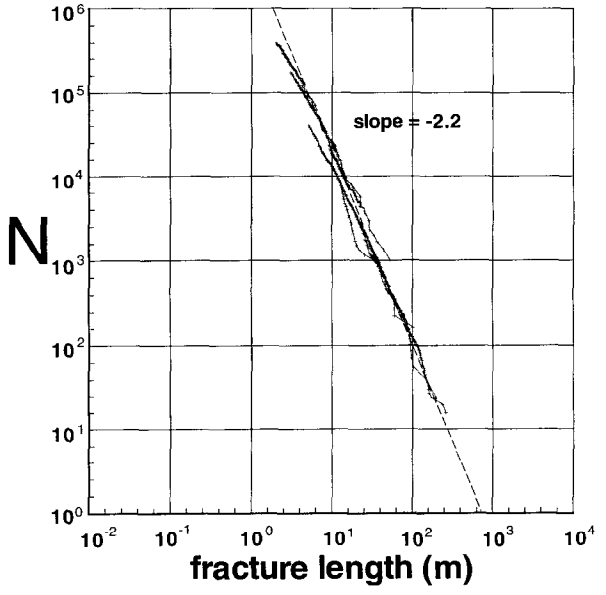

Fig. 8. Corrected cumulative frequency curves for all seven maps, after removing points affected by resolution. Together, the samples indicate a power-law cumulative frequency distribution over two orders of magnitude, with an exponent (slope of the graph) of −2.2.

envelope to the curves. By repeating the procedure with lines of different slopes the best-fit slope can be determined. This method gave a best-fit slope of −2.1, which is in good agreement with the slope of −2.2 determined from the corrected samples. This best-fit envelope line is shown in Fig. 6.

Fracture map properties and self-similarity

On the cumulative distribution plot of Fig. 6, a slope of −2.0 indicates strict self-similarity. Strict self-similarity is here used in the sense that pictures of the system at different scales should be qualitatively indistinguishable from each other or, in quantitative terms, that samples at different scales should share the same statistical properties. Thus, in a strictly self-similar system, fracture trace-length distributions of individual maps, normalized with respect to scale (i.e. observation height), should be statistically identical. A slope of −2.1 suggests that the fracture trace-length distribution in Hornelen is not self-similar in this strict sense.

Self-similarity can be tested by other means. A log–log plot of the trace-length distribution modes from the maps vs observation height (Fig. 9a) shows a power-law distribution with a slope of 0.8, while a log–log plot of apparent density (defined as total observed trace length per unit area) vs observation height (Fig. 9b) shows a slope of −0.7. The expected slope on such plots for a self-similar distribution of fracture trace lengths can be simply deduced. If self-similar, individual sample trace-length modes normalized with respect to observation height (which represents scale) should be constant, and thus the slope on a log–log plot of length mode vs observation height should be 1.0. Similarly, the normalized apparent density should be constant so that the slope

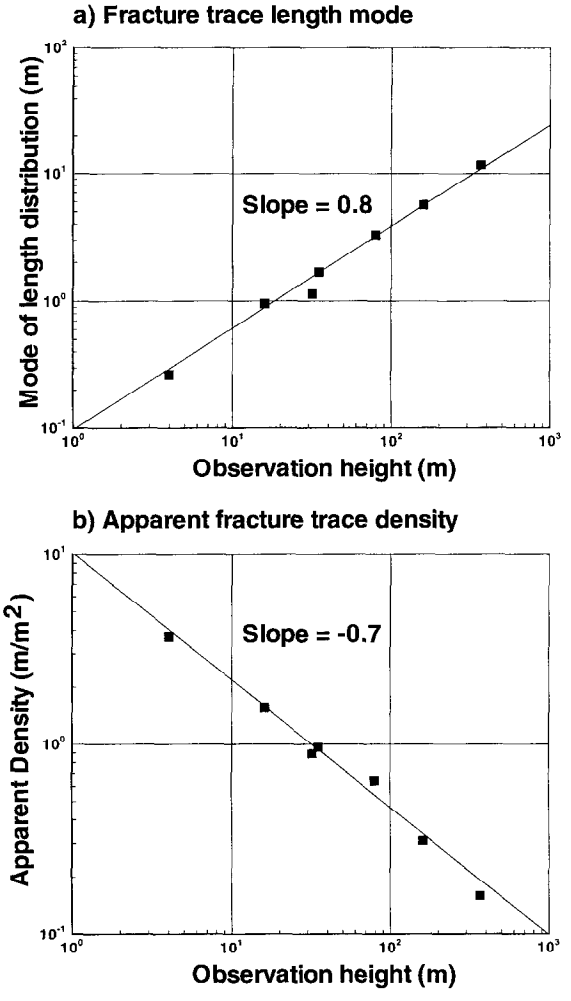

Fig. 9. (a) Length mode (mean of log length) and (b) apparent fracture trace density vs observation height for maps 1–7. Both indicate power-law behaviour which deviates from the strictly self-similar cases.

of apparent density vs observation height should be −1. The slopes of the plots in Fig. 9 differ significantly from these values and thus are consistent with the previous conclusion that the fracture system of Hornelen is not strictly self-similar.

The power laws for the cumulative trace-length distribution (exponent −2.1) and the map trace-length modes (exponent 0.8) indicate that the smaller-scale (lower resolution) maps lack relatively long fractures compared to the larger-scale (higher resolution) maps, compared to a strictly self-similar system. In addition, the power law relating apparent density and observation height (exponent −0.7) indicates that fracture densities in the small-scale (low resolution) maps are larger than expected. These features can be visually detected by comparing the small- and large-scale maps in Fig. 3.

Upper and lower cut-offs to the power-law length distribution

The analysis of the trace-length data from all maps suggests a power-law cumulative frequency distribution of fracture trace lengths with an exponent of −2.1. In

nature, such power-law distributions have upper and lower cut-offs, beyond which the power law is not valid. If such distributions are to be used in a predictive sense, it is important to identify these cut-offs. Figures 6 & 8 show a good approximation to power laws over a scale range of around two orders of magnitude, but the power law could be valid over a much wider scale range which can be evaluated semi-qualitatively. Assuming a small observation height of 2 cm, the observed fracture trace-length distribution would be expected to show a mode of 2.9 cm (Fig. 9a) and a density of 51 m/m^2 (Fig. 9b). However, reducing observation height by looking at the rock outcrop through a hand-lens does not reveal this quantity of short fractures. In fact, on this scale very little is seen in areas between fractures visible at the hand-mapping scale. Thus, taking into account that there are likely to be some truncation effects in the length distribution from map 1, the lower cut-off for the power-law length distribution lies somewhere in the region of 1 m. Although it is probable that many micro-fractures on the scale of the rock grains exist, the above suggests that they need not belong to the same power-law distribution as the data presented here.

To check the validity of the power law towards longer fracture traces, two additional maps were created from the state aerial photographs (observation height approximately 3000 m). One map was created by enlarging the aerial photograph of the study region, resulting in fewer but longer fracture traces compared to map 7. A second map covering an area of 48 km^2 was created from a mosaic of reduced photographs with markedly reduced resolution. The trace-length distributions of these two additional maps are plotted in Fig. 6 (open symbols). These distributions fall close to, and slightly below, the best-fit line of slope -2.1. They therefore support the conclusion that the slope of the log–log cumulative distribution for the parent population is steeper than -2.0, and lies sufficiently close to the line of slope -2.1 to allow extension of this power law to a scale of 3 km. Finally, at scales comparable with the size of the present-day Hornelen basin, the power law predicts that the number of fractures per km^2 of 20 km length or greater is 0.002, corresponding to about two such fracture traces in the whole basin. This is consistent with observations because lineaments on aerial photographs with a length of 20 km or more, that could represent large-scale joint zones, are very few. Thus, it seems that the power-law fracture-length distribution may be valid for at least three or four orders of magnitude, with a lower cut-off estimated at around 1 m.

ANALYSIS OF RESOLUTION

Observation height and fracture trace length

The seven fracture trace maps show that at greater observation heights the resolution cut-off occurs at longer trace lengths, suggesting a general correlation between a fracture's trace length and the strength of its visual signature. The observations on trace lengths and apparent density can be used to quantify these resolution effects.

From the distribution of cumulative frequency per km^2 (Fig. 6), we have:

$$N(l) \propto l^{-2.1} \tag{3}$$

where $N(l)$ is the number of fractures per km^2 with length greater than l. The corresponding discrete frequency distribution is obtained by differentiating the cumulative frequency with respect to length (e.g. Jackson and Sanderson, 1992):

$$f(l) \propto l^{-3.1} \tag{4}$$

where $f(l)$ is the discrete frequency of fractures of length, l, per km^2.

As there is a correlation between a fracture trace's length and its visual signature, the resolution cut-off can be expressed in terms of a critical fracture trace length, l_c, which is the shortest fracture trace always visible at observation height H. Integrating frequency per km^2 times length over an interval bounded by this lower cut-off (l_c) and an upper cut-off related to the size of the area covered (l_b) gives an approximation of the observed fracture trace density of a given map (apparent density), where the apparent density, S, is defined as total fracture trace length per km^2:

$$\begin{aligned} S &= C \int_{l_c}^{l_b} l^{-3.1}\, l \, \mathrm{d}l \\ S &= \frac{C}{1.1}\left[l_c^{-1.1} - l_b^{-1.1}\right] \end{aligned} \tag{5}$$

where C is a constant. Because l_b is large compared to l_c, density, S, can be approximated by the expression:

$$S \propto l_c^{-1.1}. \tag{6}$$

Observations (Fig. 9b) show that apparent density and observation height, H, are related by:

$$S \propto H^{-0.7}. \tag{7}$$

Thus, from equations (6) and (7):

$$l_c \propto H^{0.6}. \tag{8}$$

Turning equation (8) around gives an expression for the critical observation height of a fracture trace of length, l, i.e. the maximum observation height at which the trace is always discernible:

$$H_c(l) \propto l^{1.6}. \tag{9}$$

The exponent in equation (9) is greater than 1 and this implies that the visual signature strength grows faster than fracture length. This means that with increasing

observation height, fractures which are increasingly shorter with respect to map size become visible, so that a larger 'window' of the parent length population is observable. This is consistent with the observations from the maps: an increase in the apparent fracture trace density with H occurs because a greater range of fracture lengths are sampled at greater observation heights.

A model for resolution effects

The quantitative relationship between critical observation height and fracture trace length (equation 9), and the underlying discrete fracture trace-length frequency distribution (equation 4) provides a basis for investigating resolution effects in individual maps. To do this, a statistical model was created to simulate the effects of resolution on a parent power-law trace-length distribution, and the results are compared to the observed length distributions from individual maps. A frequency distribution for a power-law fracture trace-length population is created using equation (4). Each length is then assigned a critical observation height, H_c, using equation (9). In practice, fractures of the same length do not have exactly the same critical observation height, H_c. Thus, in the model, for a group of fractures with lengths in the small interval $l \pm \delta l$, H_c is allowed to vary according to a log-normal distribution with mean, H_c, and a standard deviation, s. Given an observation height, H, the model determines the frequency distribution of observable fracture traces, i.e. those for which H_c is greater than H.

Figure 10 shows an example of the model results in the form of cumulative frequency distributions for different standard deviations, s, of the critical observation height, H_c, associated with fractures of a given length. For very small values of s, the cumulative frequency distribution of the observed sample follows the parent population distribution down to the critical length for the given observation height, after which it becomes abruptly horizontal. The sample mode lies on or very close to the parent population trend. However, as s increases, the cumulative distribution curve for observed traces deviates increasingly from the parent population trend, and the sample mode migrates towards shorter lengths, away from the parent population trend. The model's observed samples show acceptable fits to log-normal distributions (Kolmogorov–Smirnof test), in agreement with observations from the maps.

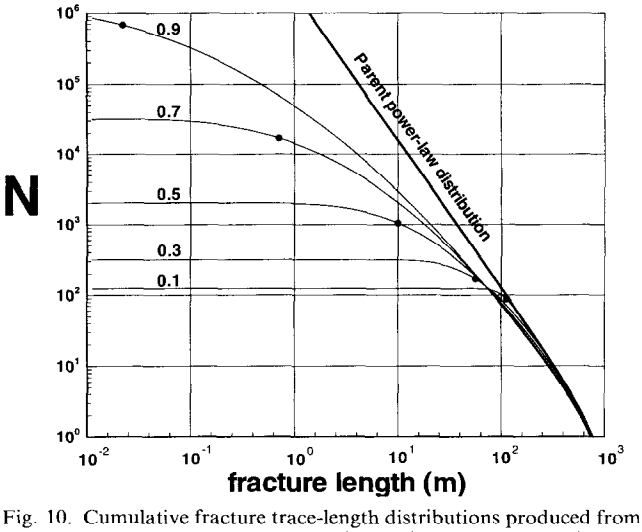

Fig. 10. Cumulative fracture trace-length distributions produced from a parent power-law trace-length distribution (thick line) by the resolution model. Each fracture trace is assigned a critical observation height. For fractures in a small length range, it assumed that critical observation heights are log-normally distributed. The curves show the resulting observed population for different values of the standard deviation, s. Filled circles, mode (mean log length) for each resultant trace-length distribution. As s increases, the curves deviate increasingly and the mode moves further away from the parent population.

As a test of the assumption that the critical observation heights, H_c, for a group of fracture traces with lengths in the small interval $l \pm \delta$ are log-normally distributed, the faintest fractures for map 2 were identified (about 17% of the sample). The length distribution of this sub-sample was found to be log-normal. By restricting the fracture traces in the model to the resolution cut-off given by the observation height for map 2 plus a small increment, it was found that this distribution could be reproduced by the model for comparable percentages of the total trace population (15–17%). This supports the assumption that the critical observation heights for fractures of a given length can be realistically modelled as log-normally distributed.

The different styles shown by the model curves in Fig. 10 are reflected in the cumulative frequency curves for the maps in Fig. 6. High resolution maps (small H) result in smooth curves with modes far to the left of the parent population, while low resolution maps (large H) show curves with sharper bends and modes closer to the parent trend. This change in style is also reflected in the proportion of the individual curves which approximate the parent population, which are short for high resolution maps and largest for the low resolution maps. This suggests that fracture zones (low resolution maps) have a more constant visual signature strength (i.e. a narrow range of critical observation heights) for a given length than the single fractures which make up the high resolution maps.

CONNECTIVITY

Fracture networks and connectivity

One of the controlling features for permeability in rock-fracture systems is the extent to which the individual fractures are linked to form continuous pathways through the rock, i.e. the fracture pattern's connectivity. When natural fracture patterns are examined from the point of view of fracture interconnection, it can be seen that they are composed of a number of groups or 'clusters' of linked fracture traces (Odling, 1992, 1995).

Here the term 'cluster' is borrowed from percolation theory, a branch of statistical physics (Stauffer, 1985). A cluster which links opposite sides of the sample area is termed a 'percolating cluster', and provides all possible paths through the fracture system across the sample region. In the case of open fractures, such percolating clusters largely control the ease with which fluids transverse the rock. The efficiency of the fracture system geometry for conducting fluid flow can thus be gauged by the proportion of the total fracture trace length which belongs to the largest cluster. When fractures are open and the rock matrix is impermeable, not all of the percolating cluster is available for fluid flow as it contains many 'dead-ends', i.e. portions of the fracture pattern which do not lie on direct pathways through the fracture system. Removing such dead-ends leaves the 'backbone', a term also borrowed from percolation theory (Stauffer, 1985). If the largest cluster of a fracture pattern is not percolating, i.e. does not connect opposite sides of the sample region, the fracture system does not possess a backbone. Although non-percolating clusters and dead-ends of percolating clusters do not provide direct routes for fluid flow, they can enhance rock permeability when the rock matrix is permeable, although such enhancement is secondary to the influence of a percolating cluster.

Apparent connectivity of the fracture trace maps

The seven fracture trace maps provide information on the connectivity of different sub-sets of the same fracture trace population. The connectivity of an individual map is thus the 'apparent' connectivity of fractures in a specific scale range determined by resolution and the size of the map area. The cluster structure of two of the maps is illustrated in Fig. 11.

In order to compare the maps at different scales, it is useful to normalize all lengths by dividing by the standardized observation heights (Table 1). This allows the geometry of the fracture patterns at different scales to be directly compared, and is equivalent to comparing information on the scale of photograph negatives. The observation height then becomes a measure of scale. Figure 12 shows that, in the maps, the number of fractures and clusters per normalized unit area increases approximately as the square root of the observation height, H. This trend corresponds to a decrease in the size of the largest cluster (identified as the proportion of the total trace length in the map belonging to the largest cluster) with observation height, H (Fig. 13). The changes in the size of the largest cluster reflect a decrease in the level of connectivity as map scale decreases. Five of the seven maps are connected both top to bottom and right to left (maps 1–5), one in one direction only (right to left, map 6) and the largest scale map (map 7) is entirely unconnected (see Fig. 11). The percolation threshold occurs when about half of the fracture trace length belongs to the largest cluster (Fig. 13). This variation in apparent connectivity with scale illustrates another way in which the maps are not strictly self-similar.

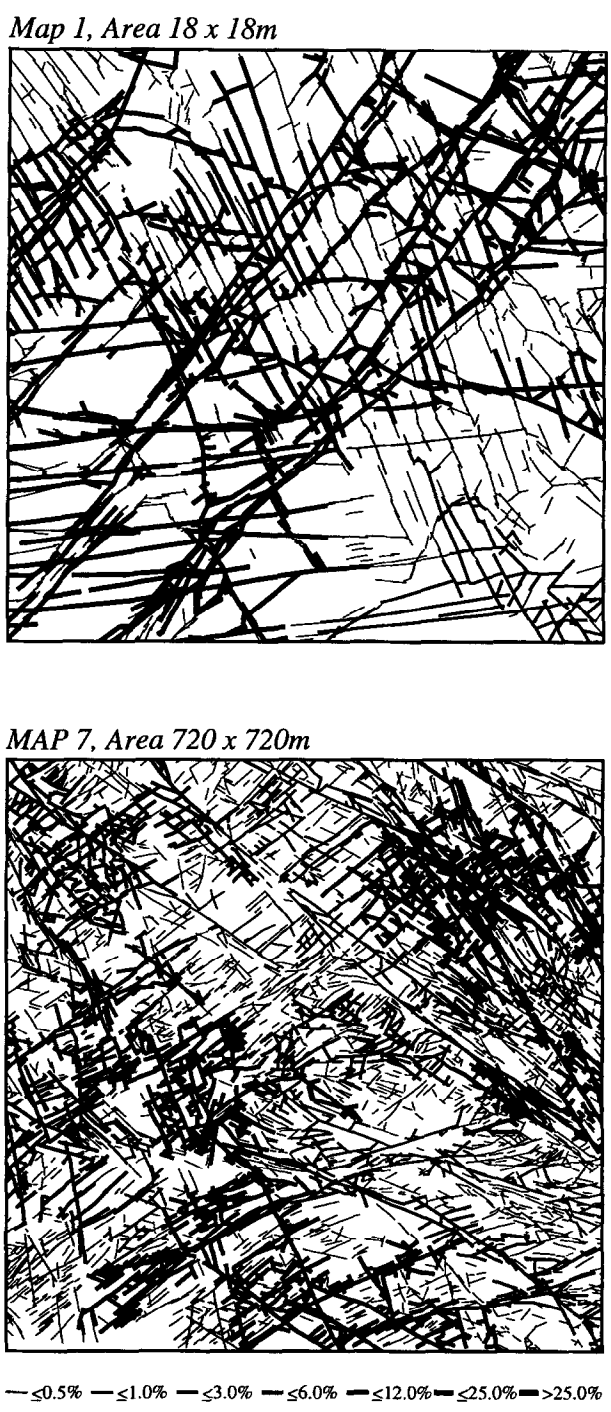

Fig. 11. Cluster structure of maps 1 and 7, illustrating the variation in connectivity with scale. A 'cluster' is a group of interconnected fracture traces. Clusters are identified by line thickness according to the proportion of the total trace length they represent. The high resolution map is well connected, i.e. the largest cluster spans the sample area, whereas the low resolution map (map 7) is unconnected, i.e. no single cluster spans the sample area.

The changes in connectivity with scale reflect changes in the fracture-length distribution. It has been shown that as scale decreases, longer fractures are not as abundant, and the apparent fracture trace density is greater than would be expected in a strictly self-similar system. When

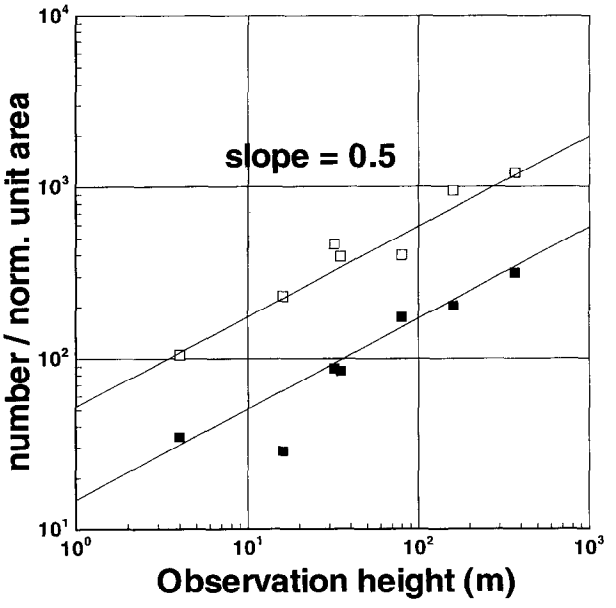

Fig. 12. Number of fractures (open symbols) and clusters (solid symbols) per normalized unit area vs observation height. Both fractures and clusters increase with increasing observation height (decreasing map scale).

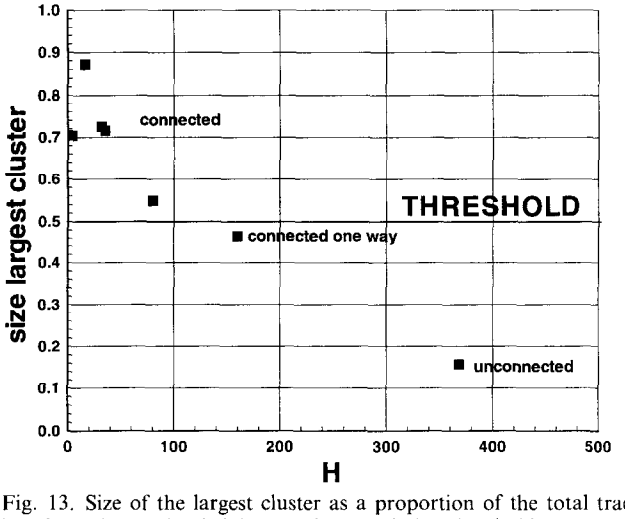

Fig. 13. Size of the largest cluster as a proportion of the total trace length vs observation height, H. The percolation threshold occurs at a cluster size of around 0.5.

all lengths are normalized with respect to observation height, this corresponds to a decrease in normalized fracture trace-length mode and an increase in normalized fracture trace density, with decreasing scale. The behaviour of connectivity in two-dimensional systems of randomly oriented and spatially distributed line segments, which provide simple models for fracture maps, has been extensively studied (e.g. Balberg and Binenbaum, 1963; Robinson, 1984; Long and Witherspoon, 1985; Berkowitz, 1995). These studies have shown that for a given line segment-length distribution increasing the number of lines results in increased connectivity. In addition, decreasing line segment length while maintaining line density, results in decreased connectivity, i.e. large numbers of short lines can be less well connected than fewer longer lines. These results suggest that, with increasing map scale, increasing normalized fracture trace density should enhance, while decreasing normalized fracture trace lengths should reduce, connectivity. Thus, these two controlling factors for connectivity are in opposition. Because observations show that the size of the largest cluster (and therefore connectivity) decreases with scale, the fracture trace-length distribution seems to be the dominant factor in this case.

The correlation between the fracture trace-length distribution parameters (mean and standard deviation of log lengths) and connectivity is shown in Fig. 14. Both plots show the same pattern; an initially steep rise in connectivity (represented by the size of the largest cluster), followed by deceasing slope of the graph with increasing fracture trace-length mode and standard deviation. The steepest part of the curve corresponds to maps that are unconnected (map 5) or connected only

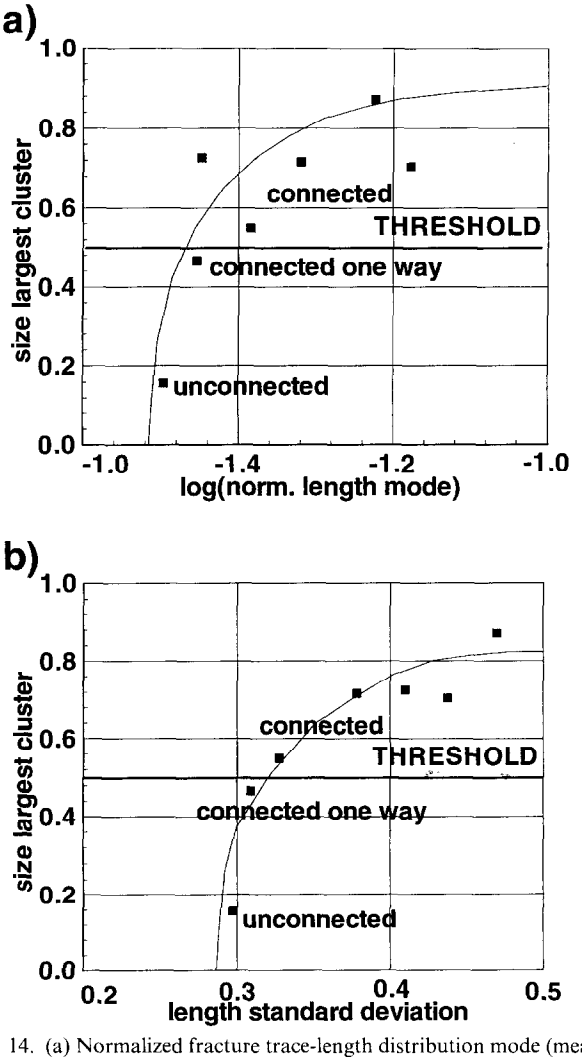

Fig. 14. (a) Normalized fracture trace-length distribution mode (mean of log lengths) and (b) standard deviation vs size of the largest cluster for maps 1–7. The system shows typical critical phenomena behaviour with rapid changes in connectivity near the threshold (transition between unconnected and connected fracture networks).

one way (map 6). This is a pattern typical of critical phenomena and has been observed in many examples of percolation (e.g. Balberg and Binenbaum, 1963; Robinson, 1984; Stauffer, 1985) where the system changes very rapidly in the region of the percolation threshold (the transition from an unconnected to a connected system). From Fig. 14, the percolation threshold for the fracture system is crossed when the largest cluster contains 0.4–0.5 of the total fracture trace length.

The nature of fracture intersections also varies with map scale. Two types of intersection exist in the maps; cross-junctions and T-junctions. T-junctions help to enhance connectivity for a given trace density as they reduce the number of dead-ends in the system. The highest resolution maps contain higher proportions of T-junctions (0.5–0.7) while low resolution maps have a lower proportion (0.1–0.3). This corresponds to maps containing mostly single traces (high resolution maps) and those containing largely fracture zones (low resolution maps). Thus, it seems that T-junctions are most common between single fractures but are less common between fracture zones.

DISCUSSION

The fracture trace-length data from the seven maps suggest that although individual maps show log-normal trace-length distributions, the assembled data sets are consistent with a power-law length distribution. A statistical model which simulates the effects of truncation (resolution) is shown to reproduce 'fall-off' from the straight-line parent population trend on a log–log cumulative distribution plot. At the highest resolutions, the combined effects of resolution and finite size effects can result in a continuous curve on the log–log cumulative distribution plot with no readily identifiable straight-line segment, even for large samples (here the maps contained over 2000 traces). The model suggests that the lack of such a straight-line segment does not necessarily rule out a power law as the underlying population distribution. In such plots, the cut-off point for resolution effects can be hard to identify. Inclusion of points still affected by resolution will tend to reduce slope estimates. It is, therefore, not surprising that slopes from individual maps are quite variable. This underlines the danger of estimating power-law exponents from single samples. To get a good estimate of the parent population, several samples at different scales from the same location are desirable.

The combined fracture trace-length distributions indicate a parent power-law cumulative distribution with an exponent of -2.1, which is shown to be significantly different from the strictly self-similar case of -2.0. Several workers have suggested underlying power-law length distributions for fracture and fault populations, with exponents ranging from -1.5 to -3.0 (e.g. Reches, 1986; Scholz and Cowie, 1990; Yielding *et al.*, 1992; Sornette *et al.*, 1993; Ouillon *et al.*, 1996). Strictly self-similar distributions (power laws with exponents close to -2.0) appear to be more the exception than the rule, suggesting that, in general, strict self-similarity should not be expected. The physical reason behind the power-law exponent of -2.1 for fracture lengths in the sandstones of Hornelen is not known, but may lie in the structure of the basin. It has been recently suggested that the thickness of geological layers on a range of scales from bedding to sedimentary sequences can influence fracture system geometry (Ouillon *et al.*, 1996). The Hornelen sandstones are underlain by a low-angle detachment characterized by highly sheared and altered basement rocks (e.g. Hossack, 1984; Norton, 1986; Wilks and Cuthbert, 1994). This detachment may have effectively decoupled, mechanically, the sandstones from the underlying basement rocks, so that joint development in the sandstones was largely independent of that in the basement. The original thickness of sediments in the Hornelen area is thought to be of the order of 14 km (Torsvik *et al.*, 1988; Wilks and Cuthbert, 1994). From preliminary observations of cliff surfaces, aspect ratios (width to height) of large-scale joints are between 1 and 2, i.e. not extreme. Joints which penetrate the whole of the sediment package could be expected to have lengths of around 14–20 km, which is similar to the length of the largest joints in the region observed on aerial photographs (1:50,000). It might also be expected that the effects of the thickness of the whole sediment package would be felt least by small joints, and most by basin-scale joints. Thus, the power-law exponent, which implies fewer large-scale joints than in a strictly self-similar system, may be reflecting the increasing influence of the basin thickness with increasing joint size.

The fracture maps range from well connected at large scales (high resolutions) to unconnected at small scales (low resolution). The connectivity of individual maps is sensitive to the abundance of the longer traces as these increase the chance of continuous pathways across the sample region. Connectivity therefore reflects the fact that, relative to the map area, high resolution maps have on average longer fracture traces, and a larger spread in lengths, which result in better connected networks. Although the largest scale map is apparently unconnected, the fracture system as a whole is likely to be connected, as the fracture spacing corresponds to the size of the smallest scale map, in which the fracture system is well connected.

The change in apparent connectivity with scale has, however, implications for the behaviour of fluid flow in the fracture system. From ground observations, the number of fractures in a fracture zone increases with critical observation height and therefore, from equation (9), with fracture length. Ground observations have also shown that fracture zones characterized by traces in the lowest resolution map are coherent and internally well-connected structures. Thus, it can be expected that, in the case of open fractures, the effective hydraulic conductiv-

ity of a fracture zone will correlate with the number of trend-parallel fractures in the zone. For open fractures, this therefore suggests that effective fracture zone conductivity increases with fracture length. When the rock matrix is impermeable, flow through the fractured rock mass is controlled by a combination of the conductivity of individual fractures and fracture zones and the connectivity of the fracture system. In the fracture system of Hornelen, it appears that the balance between these two factors changes with scale. For small volumes, the longer fractures are integral parts of the connected fracture structure and, as they are also the most conductive, control fluid flow. For larger rock volumes, however, long fractures are unconnected, and fluid flow will be controlled by smaller fractures that provide connecting pathways. This suggests that at a scale corresponding to the transition between connected and unconnected maps (around 300 m) there will be a change in the scaling behaviour of fluid flow. Above this scale it could be expected that the size of fractures controlling flow will remain constant, suggesting that a representative elementary volume (REV) (e.g. Long *et al.*, 1982; Neuman, 1987; Hestir and Long, 1990) may have been reached, i.e. bulk rock permeability may be independent of scale.

The fracture maps reflect two-dimensional connectivity in the plane of the sedimentary layering, whereas fluid flow in fractured rock masses depends on three-dimensional fracture connectivity. However, the fractures observed in the maps are perpendicular to the sedimentary layering, as is common in joint systems, and the connectivity of the maps is thus relevant to layer-parallel fluid flow. Where cross-layer flow is inhibited, therefore, the observed two-dimensional fracture patterns will give a good picture of three-dimensional flow. This occurs, for example, when beds are separated by impervious and less competent rocks which do not develop conducting fracture networks (such as shales). In addition, fractures tend to stop at layer interfaces (e.g. Ladeira and Price, 1981; Helgeson and Aydin, 1991), so that connections in the fracture system across these interfaces are restricted. Flow across such units is likely to be limited to a few widely spaced large fractures which cut many units. If the bedding planes do not provide significant flow channels, the connectivity observed in the plane of the unit controls the flow between such large-scale fractures. Thus, the connectivity observed in the plane of the layering can have significant meaning for three-dimensional flow.

CONCLUSIONS

The series of seven maps at different scales shows that the fracture system in the sandstones of Hornelen has many properties that, while they cannot be regarded as strictly self-similar, do obey power laws which would enable properties at one scale to be predicted from observations at another. Only the orientations of the major fracture sets were found to be scale-independent. Trace-length distribution, density, connectivity and nature of junctions were all found to be scale-dependent.

The fracture traces observed at a given observation height are controlled by the nature of the fractures' visual signature. While at low observation heights (high resolution), fracture traces correspond to single fractures, at greater observation heights (lower resolutions) they represent fracture zones. Critical observation height (maximum height at which a trace can be identified) is related by a power law to fracture trace lengths. The exponent in this power law implies that visual signature strength grows faster than fracture length. As a result, the lowest resolution map samples the widest scale range, and shows the highest density of fractures relative to map size. Statistical modelling suggests that the effects of resolution are spread over a wide scale range in the higher resolution maps, and can result in a smooth curve with no discernible straight-line segment on a log–log cumulative distribution plot. Thus, a smooth curve on such a plot does not necessarily rule out a power-law distribution as the underlying population.

Together, the maps indicate a power-law fracture trace-length distribution with a slope of -2.1, significantly steeper than -2.0 which is the slope expected in a strictly self-similar system. The trace-length power-law appears to have a natural cut-off in the region of 1 m, and to extend at least three or four orders of magnitude. The exponent in the fracture trace-length power-law implies that long fractures are less abundant than in a strictly self-similar system. This is expressed in the maps where long fractures in the small-scale (low resolution) maps are less abundant than long fractures in the large-scale (high resolution) maps. This has consequences for connectivity which, in the maps, decreases with decreasing scale. Although the smallest scale (lowest resolution) maps are unconnected, the high resolution maps indicate that large-scale fractures are connected by smaller fractures lying below the limit of resolution.

The apparent connectivity of different scale sub-sets of the fracture system has implications for the nature of fluid flow. A link between critical observation height and fracture width (reflecting the number of trend-parallel fractures in a fracture zone) implies a correlation between effective hydraulic conductivity and fracture size (trace length), in the case of open fractures. In this case, flow will be dominated by the largest fractures that form connected structures across the region of interest. The nature of connectivity therefore suggest that a scale exists beyond which the fractures controlling flow are scale-independent. The fracture maps suggest that this scale occurs at sample area sizes of around 300 m in the sandstones of Hornelen.

Acknowledgements—The work was carried as part of a project under the EEC 3rd Frame work, Joule II programme, and was 50% funded by the EEC programme and 50% funded by IBM. Truls Løtvedt took the aerial photography and Julie Roden assisted in the field. The author is grateful to Bremanger Kommune for permission to paint reference

crosses on the rock surface. The author would also like to thank the other partners in the project from the Fault Analysis Group of Liverpool University (U.K.), GEUS (Denmark) and BRGM (France) for helpful discussions and constructive criticism. The manuscript was improved by suggestions from two referees, Graham Yielding and Randall Marrett.

REFERENCES

Balberg, I. and Binenbaum, N. (1963) Computer study of the percolation threshold in a two-dimensional anisotropic system of conducting sticks. *Physical Review* **B28**, 3799–3812.

Berkowitz, B. (1995) Analysis of fracture network connectivity using percolation theory. *Mathematical Geology* **27**, 467–483.

Billaux, D., Chilès, J. P., Hestir, K. and Long, J. (1989) Three-dimensional statistical modelling of a fractured rock mass—an example from the Fanay-Augeres mine. *International Journal of Rock Mechanics and Mining Science & Geomechanics Abstracts* **26**, 281–299.

Burnside, C. D. (1979) *Mapping From Aerial Photographs*. Granada Publishing, London.

Cheeney, R. F. (1983) *Statistical Methods in Geology*. George Allen & Unwin, London.

Cox, D. R. and Oakes, D. (1984) *Analysis of Survival Data*. Chapman & Hall, London.

Hancock, P. L. (1985) Brittle microtectonics: principles and practice. *Journal of Structural Geology* **7**, 437–457.

Heffer, K. and Bevan, T. (1990) *Scaling Relationships in Natural Fractures—Data, Theory and Applications*. Society of Petroleum Engineers Reprint No. 20981.

Helgeson, D. E. and Aydin, A. (1991) Characteristics of joint propagation across layer interfaces in sedimentary rocks. *Journal of Structural Geology* **13**, 897–911.

Herbert, A. W. and Splawski, B. A. (1990) A prediction of flows to be measured in the Stripa D-hole experiment, an application of the fracture network approach, p. 72. AEA R&D report 0024.

Hestir, K. and Long, J. C. S. (1990) Analytical expressions for the permeability of random two-dimensional Poisson fracture networks based on regular lattice percolation and equivalent media theories. *Journal of Geophysical Research* **95B**, 21565–21581.

Hossack, J. R. (1984) The geometry of listric growth faults in the Devonian basins of Sunnfjord, W. Norway. *Journal of the Geological Society, London* **141**, 629–637.

Jackson, P. and Sanderson, D. J. (1992) Scaling of fault displacement from the Badajoz–Cordoba shear zone, SW Spain. *Tectonophysics* **210**, 179–190.

Ladeira, F. L. and Price, N. J. (1981) Relationship between spacing and bed thickness. *Journal of Structural Geology* **3**, 179–183.

La Pointe, P. R. and Hudson, J. A. (1985) Characterization and interpretation of rock mass joint patterns. *Geological Society of America Special Publication* **199**.

Lindsay, R. W. and Rothrock, D. A. (1995) Arctic sea ice leads from advanced very high resolution radiometer images. *Journal of Geophysical Research* **100C**, 4533–4544.

Long, J. C. S., Remer, J. S., Wilson, C. R. and Witherspoon, P. A. (1982) Porous media equivalents for networks of discontinuous fractures. *Water Resources Research* **18**, 645–658.

Long, J. C. S. and Witherspoon, P. A. (1985) The relationship of interconnection to permeability in fracture networks. *Journal of Geophysical Research* **90B**, 3087–3098.

Mæhle, S. (1975) Devonian conglomerate–sandstone facies relationships and their paleogeographic importance along the margin of the Hornelen basin, between Storevann and Grøndalen, Sunnfjord, western Norway. M.Sc. thesis, University of Bergen.

Neuman, S. P. (1987) Stochastic continuum representation of fractured rock permeability as an alternative to the REV and fracture network concepts. In *Proceedings of the 28th U.S. Symposium on Rock Mechanics, Tucson, U.S.A.*, pp. 533–561. A. A. Balkema, London.

Norton, M. G. (1986) Late Caledonian extension in western Norway: a response to extreme crustal thickening. *Tectonophysics* **5**, 195–204.

Nur, A. (1982) The origin of tensile fracture lineaments. *Journal of Structural Geology* **4**, 31–40.

Odling, N. E. (1992) Network properties of a two-dimensional natural fracture pattern. *Pure and Applied Geophysics* **138**, 96–114.

Odling, N. E. (1995) The development of network properties in natural fracture patterns, an example from the Devonian sandstones of western Norway. In *Fractured and Jointed Rock Masses*, eds L. R. Myer, N. G. W. Cook, R. E. Goodman, C. Tsang and F. Tsang, pp. 35–41. A. A. Balkema, London.

Ouillon, G., Castaing, C. and Sornette, D. (1996) Hierarchical geometry of faulting. *Journal of Geophysical Research* **101B**, 5477–5487.

Pickering, G., Bull, J. M. and Sanderson, D. J. (1995) Sampling power-law distributions. *Tectonophysics* **248**, 1–20.

Press, W. H., Teukolsky, S. A., Vetterling, W. T. and Flannery, B. P. (1992) *Numerical Recipes*, 2nd edn. Cambridge University Press, Cambridge.

Price, N. J. (1966) *Fault and Joint Development in Brittle and Semi-brittle Rock*. Pergamon Press, Oxford.

Reches, Z. (1986) Networks of shear faults in the field and in experiments. In *Fragmentation, Form and Flow in Fractured Media*, eds R. Englman and Z. Jaeger, Vol. 8, pp. 42–51. Israel Physics Society.

Robinson, P. C. (1984) Connectivity, flow and transport in network models of fractured media. Ph.D. thesis, Oxford University.

Scholz, C. and Cowie, P. (1990) Determination of total strain from faulting using slip measurements. *Nature* **346**, 837–839.

Sornette, A., Davy, P. and Sornette, D. (1993) Fault growth in brittle–ductile experiments and the mechanics of continental collisions. *Journal of Geophysical Research* **98B**, 12111–12139.

Stauffer, D. (1985) *Introduction to Percolation Theory*. Taylor and Francis, London.

Steel, R. (1976) Devonian basins of western Norway—sedimentary response to tectonism and to varying tectonic context. *Tectonophysics* **36**, 207–224.

Torsvik, T. H., Sturt, B. A., Ramsay, D. M., Bering, D. and Fluge, P. R. (1988) Palaeomagnetism, magnetic fabrics and the structural style of the Hornelen Old Red Sandstone, western Norway. *Journal of the Geological Society, London* **145**, 413–430.

Van Golf-Racht, T. D. (1982) *Fundamentals of Fractured Reservoir Engineering, Developments on Petroleum Science*, Vol. 12. Elsevier, Amsterdam.

Wilks, W. J. and Cuthbert, S. J. (1994) The evolution of the Hornelen Basin detachment system, western Norway: implications for the style of late orogenic extension in the southern Scandinavian Caledonides. *Tectonophysics* **238**, 1–30.

Yielding, G., Walsh, J. and Watterson, J. (1992) The prediction of small-scale faulting in reservoirs. *First Break* **10**, 449–460.